Journal of Power Sources 248 (2014) 685–689

Contents lists available at ScienceDirect

Journal of Power Sources

journal homepage: www.elsevier.com/locate/jpowsour

Short communication

The effect of local structure on ionic conductivity of apatite-type $La_{9.5}Si_6O_{26.25}$

Wei Liu [a], Takashi Tsuchiya [b], Shogo Miyoshi [c], Shu Yamaguchi [c], Kiyoshi Kobayashi [d], Wei Pan [a,*]

[a] State Key Lab. of New Ceramics and Fine Processing, School of Materials Science and Engineering, Tsinghua University, Beijing 100084, People's Republic of China
[b] Atomic Electronics Unit, MANA, National Institute for Materials Science, 1-1 Namiki, Tsukuba, Ibaraki 305-0044, Japan
[c] Department of Materials Engineering, The University of Tokyo, 7-3-1 Hongo, Bunkyo, Tokyo 113-8656, Japan
[d] Advanced Materials Processing Unit, National Institute for Materials Science, 1-2-1 Sengen, Tsukuba, Ibaraki 305-0047, Japan

HIGHLIGHTS

- Apatite-type $La_{9.5}Si_6O_{26.25}$ is synthesized via a sol–gel process.
- Sintering temperature for preparation of dense sample can be lowered to 1500 °C.
- Samples have an increased conductivity with sintering temperature.
- Local relaxation of $[SiO_4]^{4-}$ tetrahedral results in a fast ion conduction pathway.
- Sample sintered at 1650 °C exhibits the conductivity of 2.70×10^{-2} S cm^{-1} at 800 °C.

ARTICLE INFO

Article history:
Received 10 July 2013
Received in revised form
22 September 2013
Accepted 4 October 2013
Available online 12 October 2013

Keywords:
Solid oxide fuel cells
Apatite
Sintering temperature
Ionic conductivity
Raman spectroscopy

ABSTRACT

Lanthanum silicate $La_{9.5}Si_6O_{26.25}$ (LSO) with an apatite-type structure has been synthesized via a sol–gel process. The microstructure and ionic conductivity of such samples have been evaluated as a function of sintering conditions by X-ray diffraction, scanning electron microscopy, Raman spectra and AC impedance spectroscopy. The result shows that dense pellet LSO of relative density higher than 95% with pure apatite phase can be obtained at low sintering temperature of 1500 °C. The samples exhibit an increased conductivity with sintering temperature, owing to grain size effect as well as local modulation of the $[SiO_4]^{4-}$ tetrahedra. LSO sintered at 1650 °C exhibits the highest ionic conductivity of 2.70×10^{-2} S cm^{-1} at 800 °C. Probed by Raman spectroscopy, the local relaxation of the $[SiO_4]^{4-}$ tetrahedra in LSO, tuned by sintering temperature, contributes to a fast conduction pathway for interstitial oxide ions accompanying with low activation energy, which results in a high ionic conductivity.

1. Introduction

Over the past few decades, enormous effort has been devoted to develop solid oxide fuel cell (SOFC) as a promising clean and high efficient energy conversion device. Current issues especially drawing attention for further development of SOFC are related to lowering operation temperatures to intermediate/low temperature range (<700 °C) in order to achieve reduced cost, increased stability, as well as extended lifetime [1,2]. Study of a novel electrolyte that provides fast ion conduction across the electrolyte and electrode/electrolyte interfaces with negligible electronic conductivity at intermediate/low temperatures is a significant challenge, which is expected to result in a reduction in operating temperature. High stability in both oxidizing and reducing environments, good mechanical properties and compatibility with electrodes are also the requirements for the solid electrolytes for SOFC [3,4].

Among variety of oxide electrolyte materials, a new ion conductors that crystallizes in apatite structure with a general formula of $La_{9.33+x}(SiO_4)_6O_{2+1.5x}$ have been extensively investigated due to their superior ionic conductivity at moderate temperatures higher than conventional materials such as yttria-stabilized zirconia (YSZ) and various kinds of doped ceria (CeO_2). Additionally, the apatite-

* Corresponding author. Tel.: +86 10 62772858; fax: +86 10 62771160.
E-mail address: panw@mail.tsinghua.edu.cn (W. Pan).

0378-7753/$ – see front matter © 2013 Elsevier B.V. All rights reserved.
http://dx.doi.org/10.1016/j.jpowsour.2013.10.011

type electrolyte attracts future application in SOFC due to its high oxide ion transference number (>0.9) over a wide range of oxygen partial pressures, moderate thermal expansion coefficients and good mechanical properties [5–10]. However, the difficulties of the apatite-type oxides in preparing dense ceramics that require high sintering temperature (>1700 °C) and extensive holding time, limit their application as an SOFC electrolyte. In addition, the easy impurity phase formation of lanthanum silicate group also acts as the hindrance for their commercialization [11,12]. Therefore, considerable attention has been paid to the development of novel synthetic method to prepare pure oxyapatite phase at low sintering temperature [5,13]. Recently, one of smart approaches reported by Kobayashi et al. shows a water-based sol–gel synthesis to obtain pure apatite-type lanthanum silicate bulks [5].

Acting as the predominant conduction mechanism, an interstitial oxide ion conduction has been proposed for the oxyapatites, which is different from the oxygen vacancy conduction in point defect-type oxide ion conductors such as YSZ and doped CeO_2 [14–18]. Some atomistic simulation reports have predicted that the interstitial oxygen sites are accommodated at both periphery of the one dimensional (1D) lanthanum-oxide ion channels and oxide ions close to the oxygen site belonging to the tetrahedron unit of $[SiO_4]^{4-}$ [16–18]. Due to a positive dependency of the ionic conductivity on the interstitial oxide ion concentration, excess La_2O_3 is added into this apatite-type structure to increase oxide ion concentration, which results in a higher ionic conductivity. Assisted by a considerable relaxation of the SiO_4 tetrahedra to form a temporary unit of "SiO_5", the interstitial oxygen ions migrate via complex sinusoidal-like pathway along *c*-axis in the oxyanion 1D channel. Such mechanism suggests a possible positive effect of local correlative relaxation by tilting and rotation of the SiO_4 tetrahedra on the pathway of interstitial oxygen ions and resultant enhanced ionic conductivity in the apatite-type materials [10,12,19,20].

In the present study, the authors focus on the effect of sintering temperature on the local modulation of the $[SiO_4]^{4-}$ tetrahedra in lanthanum silicate $La_{9.5}Si_6O_{26.25}$ prepared by a sol–gel synthesis, and the resultant influence on the ionic conductivity of LSO. This work is mainly investigated by phase and micromorphology characterizations, electrical conductivity and Raman analyses.

2. Experimental

$La_{9.5}Si_6O_{26.25}$ powders are synthesized based on a sol–gel process with raw materials of lanthanum nitrate hexahydrate ($La(NO_3)_3\cdot 6H_2O$, 3 N, Wako Pure Chemical Industry Inc., Japan), amorphous silicon dioxide (SiO_2, 3 N, specific surface area: 200 $m^2\ g^{-1}$, Wako Pure Chemical Industry Inc., Japan) and citric acid (Reagent grade, Wako Pure Chemical Industry Inc., Japan). $La(NO_3)_3\cdot 6H_2O$ is dissolved in distilled water and the concentration of La^{3+} in the solution is determined by the chelatometric titration method in advance. Xylenol orange (Dojindo Co., Japan), ethylenediamine-*N*,*N*,*N*′,*N*′-tetraacetic acid disodium salt aqueous solution (EDTA-2Na, 0.1 M titrant, Dojindo Co., Japan) and hexamethylenetetramine (Reagent grade, Wako Pure Chemical Industry Inc., Japan) are used as indicator, chelating agent and pH buffer. In order to comparison, two kinds of solvents are used: one is the mixture of deionized water and ethanol (the volume ratio of water to ethanol is 1:4) and another is pure deionized water. The La^{3+} concentration is controlled to about 0.5 M. Then, citric acid with the same molar as $La(NO_3)_3\cdot 6H_2O$ is dissolved in the solution. After a transparent solution is obtained by vigorous stirring, a stoichiometric amount of SiO_2 powder is added. A viscous gel is then obtained by stirring at 80 °C, which is subsequently calcined at 900 °C for 3 h. The as-synthesized powders are then ground and sieved to 400 meshes, isostatically cold-pressed under 200 MPa to shape into pellets and disks, and sintered either at 1600 °C in air for 6 h or at 1450, 1500, 1550, 1600 and 1650 °C for 10 h. One of the samples is sintered at 1650 °C for 1 h, followed by the annealing at 1500 °C for 96 h.

A powder x-ray diffraction (XRD, M18XHF, MacScience, Japan) is conducted to identify the phase. The morphology of LSO samples is examined by scanning electron microscopy (SEM, JSM-7001F, JEOL, Japan). Raman spectroscopy is performed using NRS-5100 Raman microscope (Jasco, Japan). The total conductivities of the samples are investigated by both 2- and 4-probe AC impedance spectroscopy (Combination of the potentio/galvanostat with the impedance Analyzer, Solartron 1260 and 1287, UK) over the frequency range of 0.01 Hz–8 MHz, in the temperature range of 200–800 °C in air, using Pt electrode.

3. Results and discussion

3.1. Morphological and structural analysis

As shown in Fig. 1, the LSO samples prepared by the precursor solvent with the mixture of H_2O and ethanol (H_2O:ethanol = 1:4, vol. ratio) sintered at the temperatures from 1450 °C to 1650 °C for 10 h, demonstrate highly pure apatite phase without any impurity phase. In contrast, the sintered sample prepared using the precursor solvent of pure H_2O yields the impurity phase of La_2SiO_5, which indicating that the LSO powder synthesized using mixed solvent of H_2O and ethanol is more homogenous due to a better dispersion of the components by the adding of ethanol. Table 1 shows the relative densities of LSO sintered at different conditions measured by Archimedes method, demonstrating that the samples sintered at the temperature range of 1500–1650 °C for 10 h qualify the necessary requirements of a relative density of higher than 95% for use of solid electrolyte in the application of SOFCs. While, the LSO sample sintered at 1450 °C for 10 h has rather low relative density. In addition, it can be seen from Fig. 1 that the impurity of La_2O_3 has started to appear in the sample sintered at 1650 °C then by post-annealing at 1500 °C for long time of 96 h. It is particularly notorious that long-term heat treatment of the apatite-type lanthanum silicate is easy to result in the side effect in terms of

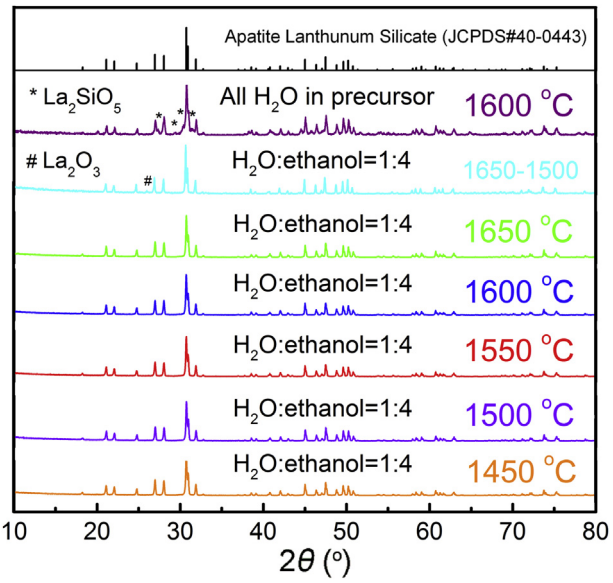

Fig. 1. Powder XRD patterns for LSOs sintered at various temperatures, together with the samples prepared by different precursor solvents.

Table 1
Relative densities of LSOs sintered at various temperatures and holding time.

Temperature (°C)/holding time (h)	1600/6	1450/10	1500/10	1550/10	1600/10	1650/10	1650/10	1650-1500
Relative density (%)	92.5	89.2	95.0	95.2	95.7	95.3	95.3	95.5

reduction to SiO by volatilization, which produces a mixture of apatite and La_2O_3 additional phase, which probably degrades the electrical property.

Fig. 2(a)–(f) exhibits the microstructure of thermally etched surfaces of LSO sintered at various temperatures and annealing periods. The surface micrographs clearly indicate that all the specimens are dense and a few pores can be observed, indicating good agreement with the relative density results in Table 1. As the sintering temperature increases from 1500 °C to 1650 °C, the average grain size of the LSO samples grows from 2 μm to 7 μm. For the sample sintered at 1650 °C then followed by additional annealing at 1500 °C for 96 h (defined as Sample 1650-1500), the prolonged annealing treatment has negligible influence on grain growth, whereas the ionic conductivity of Sample 1650-1500 is much lower than that of the one sintered at 1650 °C for 10 h (defined as Sample 1650), as shown in the following section. As show in the SEM image of Fig. 2(e), the impurity of La_2O_3 appeared in Sample 1650-1500 by long time post-annealing may segregate in grain boundaries.

3.2. Total conductivity

Typical impedance diagram of LSO sintered at 1600 °C measured at 300 °C and 400 °C by 2-probe method are shown in Fig. 3(a), together with the fitting curves. At low measurement temperatures, two capacitive semicircles in addition to the Warburg impedance, Z_w, are clearly observed in the diagram. As shown in Fig. 3(a), the semicircle at high frequency is attributed to the relaxation of the oxide ion migration in both bulk and grain boundary. The semicircle and the straight line with phase angle at low frequencies correspond to the AC response at electrode/electrolyte interface including charge transfer resistance, R_{ct}, and capacitive element parallel-connected with charge/discharge of an electric double layer, CPE (EDL), and concentration overpotential by chemical diffusion of neutral oxygen species to the charge transfer reaction site (diffusion-limited overpotential), respectively. The semicircles shift to higher frequencies with increasing measurement temperature, indicating fast relaxation of oxide ion migration in time domain due to increased conduction. As shown in the inset of Fig. 3(a), in the 4-probe AC impedance diagram, both the bulk and grain boundary resistance can be determined more exactly, in comparison to the 2-probe method, due to the negligible influence of the interface/electrode impedance. The data of the 4-probe AC impedance diagram is from our previous work [21] that provides detailed description about the 4-probe AC impedance measurement. Fig. 3(b) demonstrates that the conductivity of LSO measured by 4-probe method is identical to the one measured by 2-probe method.

The temperature dependence of total conductivity for LSO sintered at various conditions is depicted in Fig. 4(a) as an Arrhenius plot, demonstrating a single conduction mechanism for the total conductivity, due to absence of apparent curvature in the plots. It also can be seen that the LSO samples sintered for 10 h have higher conductivity than that of 8YSZ (self-prepared by solid-state reaction method) at intermediate/low temperatures, due to their lower activation energy, which indicates the superiority of apatite silicates for the use as solid electrolyte in the intermediate/low SOFC.

The temperature dependence of the electrical conductivity of LSO sintered at various conditions is shown in Fig. 4(a) as an Arrhenius plot of ln σT vs. 1000/T, together with the data of YSZ. It can be seen from Fig. 4(a), as account of the higher density, the ionic conductivity of LSO sintered at 1600 °C for 10 h is much higher than that of the one sintered at the same temperature for 6 h, while the samples sintered at temperatures from 1500 to 1650 °C for the same holding time of 10 h do not exhibit large difference in conductivity. Fig. 4(a) shows that the LSO sample sintered at 1650 °C exhibits an extremely high conductivity of 2.70×10^{-2} S cm^{-1} at 800 °C, which is three times higher than the literature value [22].

It is noteworthy that the conductivity of LSOs sintered at the temperature range of 1500–1650 °C increases with sintering temperature, even though these LSOs are of similar relative densities,

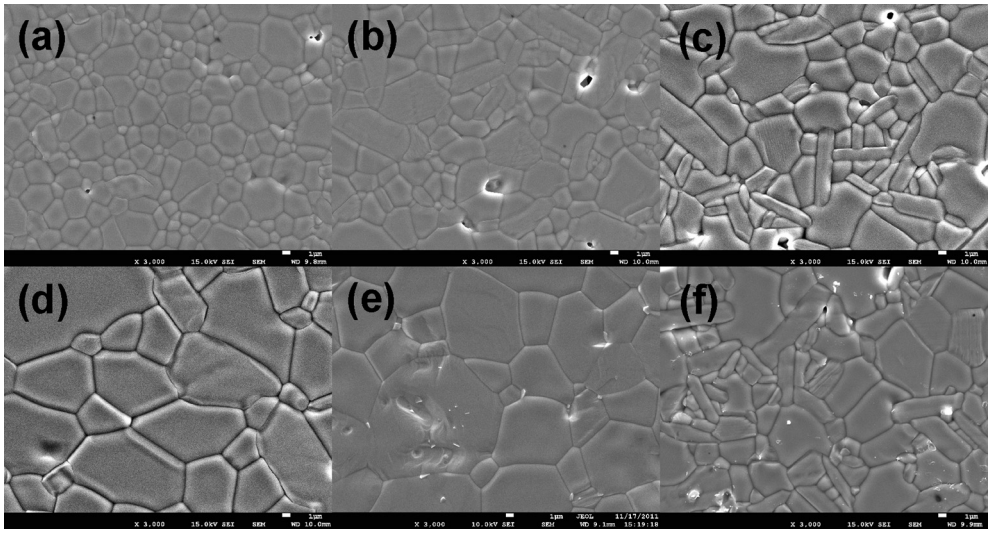

Fig. 2. SEM images of thermally etched LSOs sintered at (a) 1500 °C, (b) 1550 °C, (c) 1600 °C, (d) 1650 °C for 10 h, together with the one sintered at (e) 1650 °C for 1 h followed by post annealed at 1500 °C for 96 h and the sample sintered at (f) 1600 °C for 6 h.

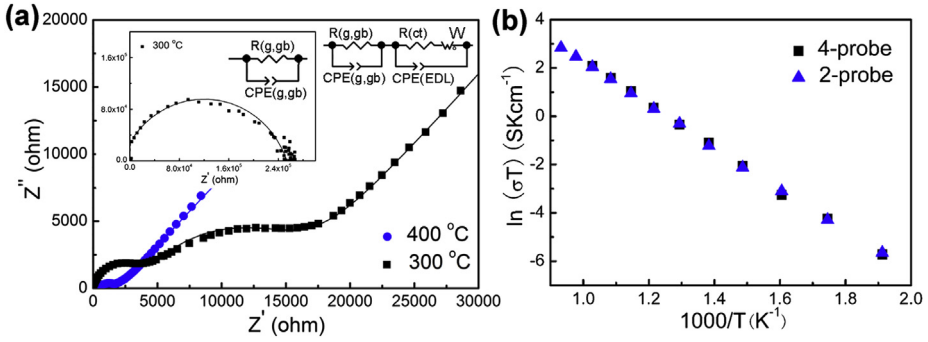

Fig. 3. (a) Impedance diagram of LSO sintered at 1600 °C measured by 2-probe method at various temperatures. The inset shows the impedance diagram measured by 4-probe method. (b) Comparison of Arrhenius plots of LSO by 2- and 4-probe methods.

for which two reasons could be deduced. One is the increased grain size with the sintering temperature, and the other is the local atomistic structure modulation. For the ceramic bulk of micro-scale grain size, as a result of the higher grain interior conductivity compared with grain boundary conductivity, the total ionic conductivity of the bulk improves with grain size that increases with sintering temperature, which is confirmed by Fig. 4(b). Fig. 4(b) shows that the conductivity of grain is higher than that of grain boundary, and when rising sintering temperature both grain interior conductivity and grain boundary conductivity enhance.

From the comparison of Fig. 2(d) and (e), we can observe that the grain sizes of Sample 1650 and Sample 1650-1500 are almost the same, which indicates that no macroscopic modulation of the grains, such as grain growth occurs when the sample was sintered at 1650 °C followed by annealing at 1500 °C. In addition, Sample 1650 and Sample 1650-1500 have the similar relative density. However, the fact that the ionic conductivity of Sample 1650-1500 is much lower than that of Sample 1650 suggests other influences on the conductivity rather than density or grain size effect. In addition, the impurity segregation in Sample 1650-1500 by long time annealing treatment may be one contribution to this conductivity reduction, especially the decrease in grain boundary. It is found that grain interior conductivity and grain boundary conductivity are both lowered by the post long time annealing. The explanation for the reduction of grain conductivity should be further studied. The occurrence of different structural modification by annealing may be a main effect. If local structural modification in atomic scale, such as coordination structure of $[SiO_4]^{4-}$ tetrahedra group and distortion of the network, takes place only at temperatures higher than 800 °C, far above the temperature range of the conductivity measurement, the local structure is quenched from the sintering or the post-annealing temperature, which may play a key role on the total conductivity of the LSO electrolyte.

3.3. Raman spectroscopy study

When the apatite-type lanthanum silicates exhibit an interstitial oxide ion conductivity, in which interstitial oxide ions migrate between the interstitial sites in La channels and the isolated $[SiO_4]^{4-}$ tetrahedra along a sinusoidal-like migration pathway, and a transient structure of "SiO_5" is suggested to form [19,23,24]. The interstitial oxide ion mechanism is made by a co-operative displacement and tilting of the $[SiO_4]^{4-}$ tetrahedron [10,12,19,20,24], which can be identified clearly as characteristic peaks of SiO_4 structure by Raman spectroscopy. Fig. 5(a) depicts the Raman spectra of LSO sintered at various temperatures, measured at room temperature, which confirms the presence of pure apatite phase without any other impurity trace, in good agreement with XRD result. In Fig. 5(a), the Raman bands around 830–870 cm^{-1} and 365–410 cm^{-1} are attributed to the symmetric stretching mode ν_1 and bending mode ν_2 of SiO_4 unit. The weak bands at 980 cm^{-1} and 525 cm^{-1} can be assigned to the asymmetric stretching mode ν_3 and bending mode ν_4, respectively [25–27].

As shown in Fig. 5(b), the intensity ratio of symmetric mode to asymmetric mode ($I(\nu_1+\nu_2)/I(\nu_3+\nu_4)$) increases with sintering temperature, which demonstrates the increase in the intensity of the symmetric stretching and bending mode, in comparison to the asymmetric mode in the apatite-type LSO structure. The change of Raman bands suggests that the $[SiO_4]^{4-}$ tetrahedra undergo a structural modification by the reduction of asymmetric arrangement. Combining the above conductivity results, as the value of $I(\nu_1+\nu_2)/I(\nu_3+\nu_4)$ rises, the ionic conductivity of LSO improves. That is, increasing sintering temperature may result in an asymmetry reduction of the $[SiO_4]^{4-}$ tetrahedra in the apatite-type materials, which takes a possibility of a more positive effect of local correlative relaxation by tilting or rotation of the $[SiO_4]^{4-}$ unit on the pathway of interstitial oxygen ions, which facilitates an effective

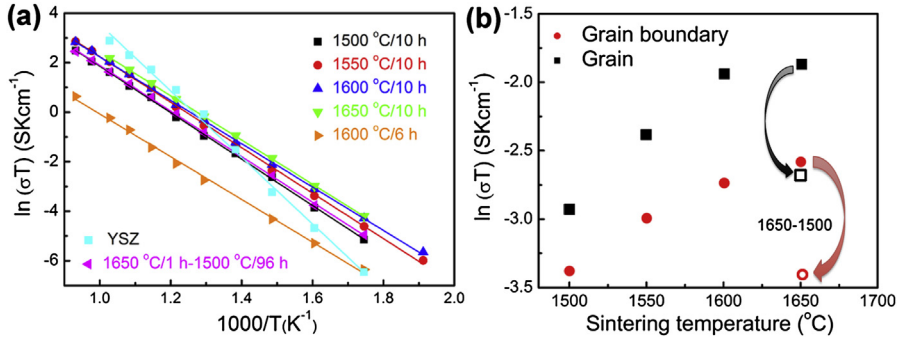

Fig. 4. (a) Arrhenius plots of LSOs sintered at various conditions, together with the data of 8YSZ. (b) Grain conductivity and grain boundary conductivity of LSO vs. sintering temperature measured at 350 °C.

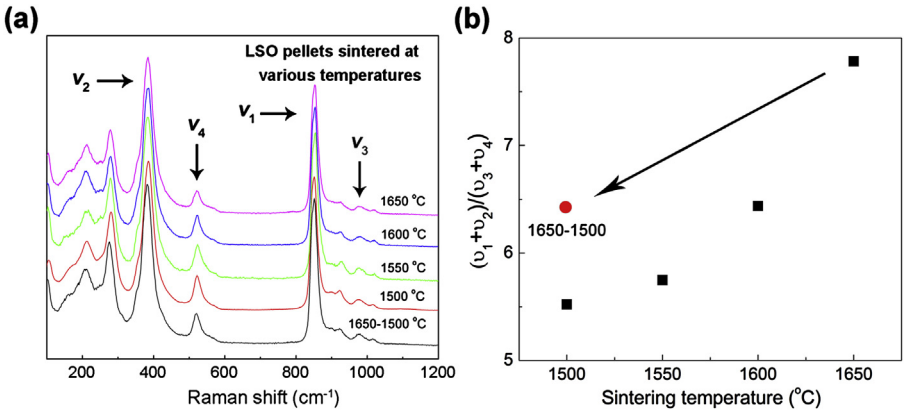

Fig. 5. (a) Raman spectra of LSOs sintered at various temperatures. (b) $I(\nu_1+\nu_2)/I(\nu_3+\nu_4)$ as a function of sintering temperature and post-annealing temperature.

Table 2
Activation energies of LSOs sintered at various conditions.

Temperature (°C)/time (h)	1500/10	1550/10	1600/10	1600/6	1650/10	1650-1500
E_a (eV)	0.809 ± 0.006	0.792 ± 0.007	0.756 ± 0.005	0.767 ± 0.009	0.770 ± 0.003	0.794 ± 0.004

pathway for interstitial oxide ions and resultantly enhances ionic conductivity [27]. Accordingly, as is evident from the results listed in Table 2, the activation energy of oxide-ion migration slightly decreases for LSO sintered at higher sintering temperature, which indicates lower energy barrier for the transport of interstitial oxygen ions from one SiO_4 unit to a neighboring one, confirming the effective pathway for interstitial oxide ions aided by the modulation of the $[SiO_4]^{4-}$ tetrahedra.

Furthermore, Fig. 4(a) also indicates that both grain conductivity and grain boundary conductivity of Sample 1650-1500 are lower than that of Sample 1650, although these two samples have similar relative density as well as grain size. The lower grain boundary conductivity of Sample 1650-1500 is due to the impurity segregated in grain boundaries. While the decreased grain conductivity may be attributable to the change of the $[SiO_4]^{4-}$ tetrahedra by the prolonged annealing treatment. We note here that the $I(\nu_1+\nu_2)/I(\nu_3+\nu_4)$ value of Sample 1650-1500 is lower than that of Sample 1650, which implies a stronger asymmetry and weaker local structural modification, resulting in a lower ionic conductivity of Sample 1650-1500. Table 2 also indicates that the activation energy of LSO sintered at 1650 °C increases from 0.770 to 0.794 eV by the post-annealing at 1500 °C, which implies a higher energy barrier for the conduction of interstitial oxygen ions and a resultant lower ionic conductivity for Sample 1650-1500. Therefore, it is evident that the local structural modification of the $[SiO_4]^{4-}$ tetrahedra governed by sintering and post-annealing temperature, in addition to relative density and grain growth, has significant impact on the ionic conductivity of the apatite-type materials.

4. Conclusions

In conclusion, this work has demonstrated the effect of sintering temperature on the phase, microstructure and ionic conductivity of the LSO electrolytes systematically, based on XRD, SEM, AC impedance spectroscopy and Raman spectroscopy. LSO sintered at low temperature of 1500 °C for 10 h has high relative density of 95%. The polycrystalline LSO body shows improved ionic conductivity as increasing sintering temperature. LSO sintered at 1650 °C shows the highest conductivity of 2.70×10^{-2} S cm^{-1} at 800 °C. In addition to the reduced grain boundary resistance by grain growth, the current results also reveal another strong impact of sintering and annealing on the ionic conductivity of LSO through the local structure modification of the $[SiO_4]^{4-}$ tetrahedra around oxide ion migration path for increased mobility.

Acknowledgments

The authors acknowledge financial support from TOYOTA MOTOR Corp.

References

[1] B. Zhu, J. Power Sources 114 (2003) 1.
[2] N.Q. Minh, Solid State Ionics 174 (2004) 271.
[3] A.C. Johnson, B.K. Lai, H. Xiong, S. Ramanathan, J. Power Sources 186 (2009) 252.
[4] A.J. Jacobson, Chem. Mater. 22 (2010) 660.
[5] K. Kobayashi, Y. Matsushita, N. Igawa, F. Izumi, C. Nishimura, S. Miyoshi, Y. Oyama, S. Yamaguchi, Solid State Ionics 179 (2008) 2209.
[6] S. Nakayama, Y. Sadaoka, J. Mater. Chem. 3 (1993) 1251.
[7] S. Nakayama, H. Aono, Y. Sadaoka, Chem. Lett. (1995) 431.
[8] J.M. Porras-Vázquez, E.R. Losilla, L. León-Reina, David Marrero-López, M.A.G. Arandaw, J. Am. Ceram. Soc. 92 (2009) 1062.
[9] E. Béchade, I. Julien, T. Iwata, O. Massona, P. Thomasa, E. Championa, K. Fukuda, J. Eur. Ceram. Soc. 28 (2008) 2717.
[10] J.R. Tolchard, P.R. Slater, M.S. Islam, Adv. Funct. Mater. 17 (2007) 2564.
[11] E. Jothinathan, K. Vanmeensel, J. Vleugels, O. Van der Biest, J. Eur. Ceram. Soc. 30 (2010) 1699.
[12] E. Kendrick, M.S. Islam, P.R. Slater, J. Mater. Chem. 17 (2007) 3104.
[13] B. Li, W. Liu, W. Pan, J. Power Sources 195 (2010) 2196.
[14] E. Kendrick, D. Headspith, A. Orera, D.C. Apperley, R.I. Smith, M.G. Francesconi, P.R. Slater, J. Mater. Chem. 19 (2009) 749.
[15] S. Beaudet-Savignat, A. Vincent, S. Lambert, F. Gervais, J. Mater. Chem. 17 (2007) 2078.
[16] J.R. Tolchard, M.S. Islam, P.R. Slater, J. Mater. Chem. 13 (2003) 1956.
[17] A. Jones, P.R. Slater, M.S. Islam, Chem. Mater. 20 (2008) 5055.
[18] M.S. Islam, J.R. Tolchard, P.R. Slater, Chem. Commun. (2003) 1486.
[19] E. Béchade, O. Masson, T. Iwata, I. Julien, K. Fukuda, P. Thomas, E. Champion, Chem. Mater. 21 (2009) 2508.
[20] J.E.H. Sansom, J.R. Tolchard, M.S. Islam, D. Apperley, P.R. Slater, J. Mater. Chem. 16 (2006) 1410.
[21] W. Liu, S. Yamaguchi, T. Tsuchiya, S. Miyoshi, K. Kobayashi, W. Pan, J. Power Sources 235 (2013) 62.
[22] Y. Higuchi, M. Sugawara, K. Onishi, M. Sakamoto, S. Nakayama, Ceram. Int. 36 (2010) 955.
[23] S.H. Jo, P. Muralidharan, D.K. Kim, Electrochim. Acta 54 (2009) 7495.
[24] L. León-Reina, E.R. Losilla, M. Martínez-Lara, S. Bruque, M.A.G. Aranda, J. Mater. Chem. 14 (2004) 1142.
[25] G. Gouadec, P. Colomban, Prog. Cryst. Growth Charact. Mater. 53 (2007) 56.
[26] E. Rodríguez-Reyna, A.F. Fuentes, M. Maczka, J. Hanuz, K. Boulahya, U. Amadore, J. Solid State Chem. 179 (2006) 522.
[27] L. Zhang, H.Q. He, H.W. Wu, C.Z. Li, S.P. Jiang, Int. J. Hydrogen Energy 36 (2011) 6862.